Kovove Mater. 51 2013 317–325
DOI: 10.4149/km_2013_5_317

The effect of process parameters on the surface form of laser engraved H13 tool steel

Ş. Kasman[1]*, I. E. Saklakoğlu[2]

[1]*Dokuz Eylul University, Izmir Vocational School, 35160 Izmir, Turkey*
[2]*Ege University, Faculty of Engineering, Department of Mechanical Engineering, 35100 Izmir, Turkey*

Received 20 January 2012, received in revised form 19 November 2012, accepted 20 November 2012

Abstract

The milling of hard materials with a complex shape using conventional methods causes many tool based problems. However, a laser assisted milling process eliminates the tool-based problem because of the small, high intensity beam used. Laser engraving, which is one of milling methods, is an effective process for the machining of difficult to machine geometries and materials like hot work tool steels. This study focuses on recast layer formation and subsurface hardness as a function of distance. Power, scan speed and frequency were employed for the investigation. The highest hardness was detected at 201 HV, which measured at 800 mm s^{-1} for scan speed and 40 kHz for frequency. XRD analysis showed that two different phases, Fe and $Fe_{2.96}Si_{0.05}O_4$, existed on the machined surfaces.

K e y w o r d s: laser engraving, microstructure, hardness, recast layer

1. Introduction

The parts with small or micro scale features [1] or a mold parts require precision machining techniques. Due to tool-based problems, the fabrication of micro-scale features by conventional methods is difficult in certain aspects. The dimensional accuracy of machined surface and the amount of removed material are the critical issues. Especially, the machining of hard metals with low flexural stiffness is limited by the machine-tool system [2]. The laser based machining techniques are the effective techniques for difficult to machine material by classical chip-removal techniques [3]. Laser-assisted precise machining methods such as milling, engraving, cutting and drilling provide a material removal without contact, and have no tool wear or cutting force [4]. In these processes, the material removal mechanism is performed by a high intensity laser beam regardless of the material hardness. This mechanism occurs in two stages: localized melting and then rapid vaporization [5]. During these stages, a heat affected zone and a re-solidified region occur very quickly. The laser transformation hardening, laser surface melting, or laser surface alloying are performed by solid-state laser in pulsed or CW modes [6]. In the laser surface hardening, the process is performed at rapid heating and cooling cycles without affecting the bulk of samples [7]. The continuous wave (CW) Nd:YAG laser has some advantages such as small spot size, higher energy density, and higher energy absorption rate in comparison to the CO_2 laser [8]. However, the pulsed lasers produce smaller heat affected zone and recast layer at machined surface [9]. Additionally, the interaction time is smaller than with the other lasers. Another essential factor in the material processing with pulsed lasers is the overlap ratio, which determines the uniformity and continuity properties of the laser treated area [6].

In the literature, there are many studies related to laser surface hardening of steel. Singh et al. [1] studied the characterization and prediction of the heat affected zone (HAZ) caused by laser heating in the laser-assisted micro-milling process of AISI H13. In addition, in order to correlate hardness with the workpiece temperature, a 3D transient finite element model for a moving Gaussian laser heat source was developed and used to calculate the temperatures produced in the

*Corresponding author: e-mail address: sefika.kasman@deu.edu.tr

workpiece by laser heating. Melkote et al. [2] studied the micro-milling of A2 tool steel. They carried out experiments to evaluate the effect of laser heating and cutting speed on the dimensional accuracy and surface finish of the grooves micro-milled in hardened A2 tool steel. In a study by Mahmoudi et al. [6], pulsed Nd:YAG laser with a maximum mean laser power of 400 W was used as the laser source for experiments on laser transformation hardening of AISI 420. The effect of the laser process parameters on the hardness and depth of the hardened area and the effect of overlap ratio on the pitting corrosion resistance of the hardened area were investigated. Leone et al. [10] performed laser marking tests on AISI 304 using a 20 W Q-switched diode pumped Nd:YAG laser in order to determine the best working parameters to obtain a given visibility. Lee et al. [11] investigated the effect of heat treatment on microstructure characteristics, such as hardness and beam scan rate, of AISI H13. They used a fiber laser with a maximum power of 200 W. Jebbari et al. [12] investigated the effect of the characteristic laser parameters (absorbed laser energy and impact diameter of the laser beam) with the characteristic parameters of the groove to estimate the energy quantity causing the thermal effected zone (TAZ). They used XC42 steel as the workpiece, and the experiments were carried out using a CO_2 laser with a maximum output power of 5 kW.

These previous experiments showed that three different parameters affected the surface roughness and depth. They also reached conclusions that the optimal values of parameters which minimized surface roughness and maximized engraving depth were not similar. Therefore, in this study, an experimental layout was constituted using the optimal value of the parameters. In this context, a series of examinations for engraved surfaces by fiber laser were performed to investigate the crater formation, recast layer and hardness as a function of distance. For this purpose, SEM, optic microscopy and XRD analyses were performed and the results discussed.

2. Laser engraving process

Laser engraving is one of the surface milling methods that provide material removal as a result of the interaction between the high intensity laser beam and the material. During the interaction, a melting and rapid vaporization mechanism occurs on the workpiece surface. The material is removed during the action of the laser pulses, which heats the material to melting and vaporization temperatures [13]. At the end of the vaporization process, a rapid solidification mechanism begins and, during this stage, a part of the material re-solidifies in a cavity. As a result of the vaporization and solidification processes, a recast layer occurs. Figure 1 shows the cavity, recast material and recast layer. In addition, a heat-affected zone, with possible micro-cracks in the material and surface damage caused by the metal droplets, is generated [13]. The re-solidification mechanism also affects the surface roughness as a result of the cavity depth.

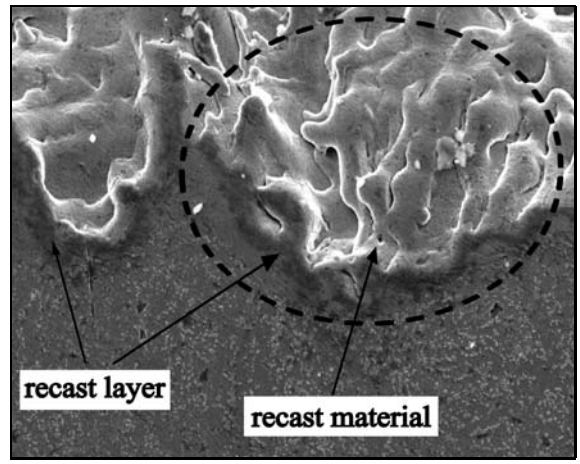

Fig. 1. The sample for cavity form, recast material and recast layer.

The performance characteristics and the response of the engraving process are the surface quality and the amount of removed material. Many parameters such as the laser power, scan speed, frequency, focal distance and fill spacing affect the response in the engraving process. Generally, the interaction of more than one parameter determines the performance characteristics but, sometimes, only one parameter has this effect. The pulse scan overlap rate occurs as a result of the interaction of more than one parameter. The pulse scan overlap rate (O_p) shown in Fig. 2 is the distance between the successive laser pulses at the same scan line. It is obvious that, when the scan speed and beam spot diameter remain constant, any increase in frequency leads to an increase in the pulse scan overlap rate (O_p). This causes an increase in the number of pulses per unit area, and thus the number of craters and cavities increases.

$$L = SS/F \Rightarrow O_\mathrm{p} = x/D = [1 - SS/(F \cdot D)] \cdot 100, \quad (1)$$

$$t_\mathrm{i} = \frac{D}{SS}, \quad E_\mathrm{d} = P_\mathrm{d} \cdot t_\mathrm{i} \rightarrow E_\mathrm{d} = \frac{P \cdot D}{A \cdot SS}, \quad (2)$$

where x is the overlap length at the x-axis, L is the center to center distance between two successive beam spots, SS is the scan speed ($\mathrm{mm\,s^{-1}}$), F is the frequency (kHz), D is the beam spot diameter (μm), t_i is the interaction time, P_d is the power density and E_d is the energy density [12, 13].

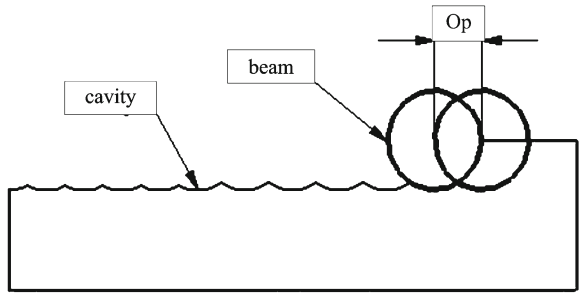

Fig. 2. The pulse scan overlap rate.

Table 1. The chemical compositions of AISI H13 (wt.%)

Element	C	Si	Mn	Cr	Mo	V	Fe
Content (%)	0.3	1	0.36%	5.54%	1.33%	0.4	Bal.

3. Experimental procedures

The workpiece material used in the engraving applications is the AISI H13. The chemical analysis of the workpiece material is given in Table 1. Samples with dimensions of 20 mm × 20 mm × 20 mm were used for examination of the subsurface.

The experimental studies were performed by using a marking machine combined with an ytterbium-doped fiber laser with a wavelength of 1064 nm and an output power of 30 W. The motion of the laser beam and the process parameters were controlled by a PC. In the experiments, the engraving test sample was stationary and mounted on an aluminum plate. Each machining area ($10 \times 10\,\mathrm{mm}^2$) was scanned 20 times at the 0° direction to achieve a deep cavity result. All the experiments were performed in standard atmospheric conditions and no assisting gas was used. Figure 3 shows the sample of the machined surface achieved at 30 W, 20 kHz, 200 mm s^{-1} and 0.03 mm.

3.1. Process parameters and test procedure

The process parameters and their values are given in Table 2. Each level of the parameters was selected within levels which provide the best and worst *Ra* and *D* value. In all tests, the focal distance and fill spacing remained constant.

The machined surface was characterized by a Mitutoyo Surftest SJ301 stylus profilometer. The subsurface was characterized by hardness distribution as a function of distance (25 μm). Before hardness tests, a cross-section of the machined surface was prepared using a standard grinding and polishing process. Finally, the polished surface was etched with 2 % Nital's reagent. Optical microscopy and scanning electron microscopy (SEM) were used to show the crater forms and investigate the recast layer, respectively. In addition, XRD analysis was used to determine the composition of the recast layer. The micro-hardness measurements of the recast layer and subsurface were taken

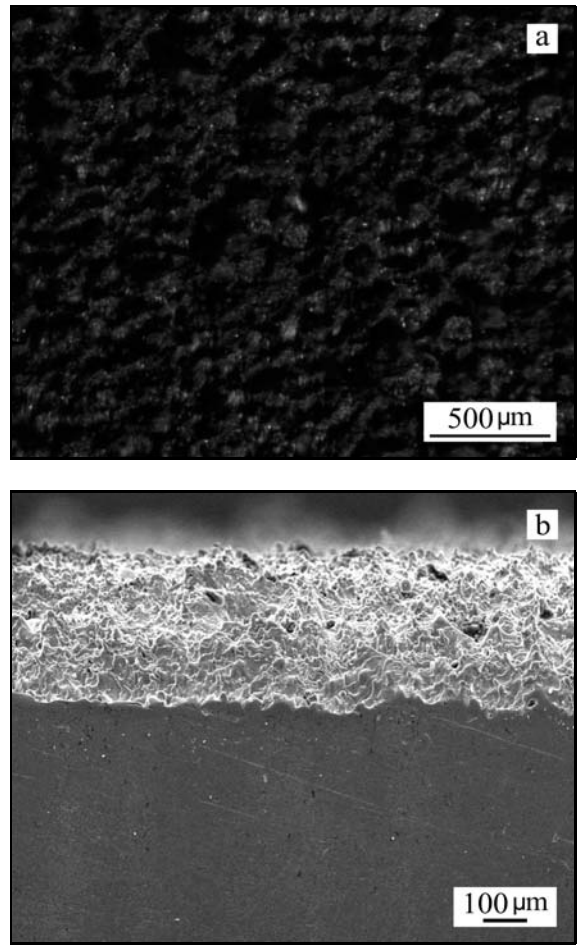

Fig. 3. The sample of machined surface at 30 W, 20 kHz and 200 mm s^{-1}: (a) top view and (b) cross section.

Table 2. The experimental design layout of engraving experiments

No.	Power (W)	Scan speed (mm s^{-1})	Frequency (kHz)	Fill spacing (mm)
1	18	200	20	0.03
2	18	200	40	0.03
3	18	800	20	0.03
4	18	800	40	0.03
5	30	200	20	0.03
6	30	200	40	0.03
7	30	800	20	0.03
8	30	800	40	0.03

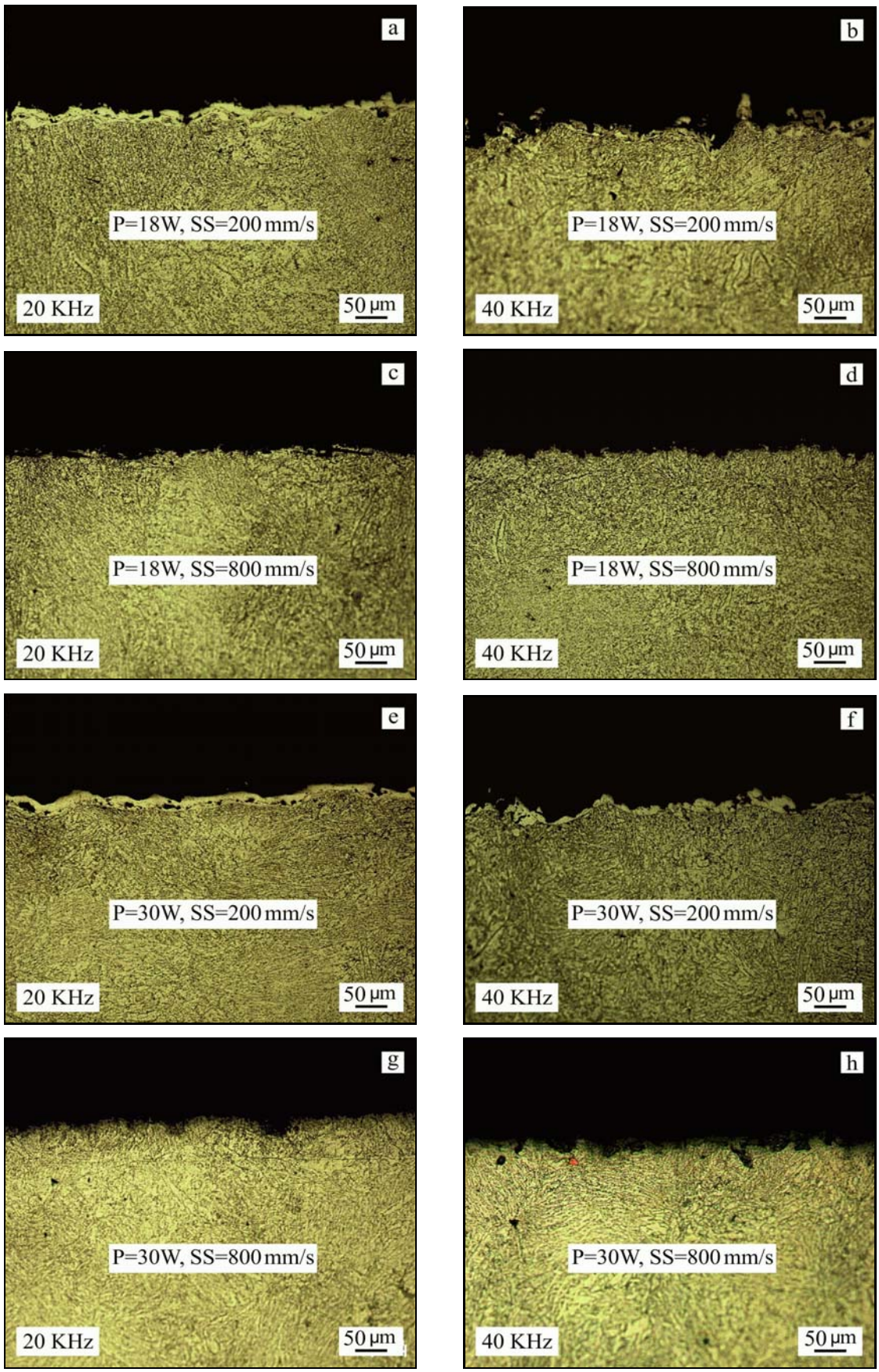

Fig. 4a–h. The effect of laser parameters on the crater formation.

using a micro Vickers hardness tester (HMV-2 Shimatzu) with a load of 10 g and for 10 s.

4. Results and discussions

In order to evaluate the effect of the laser engraving parameters on the hardness of the subsurface and crater formation on the machined surface, an experimental layout, shown in Table 2, was constituted. The results of the analyses are discussed in the following sections.

4.1. Microstructure examinations

To evaluate the crater formation, two different examinations were performed. The first examination was performed by optical microscopy. Figure 4 shows the crater depth and surface form. As seen in Fig. 4, the crater depth and surface damage increase with a decrease in laser power at the constant scan speed. This is due to heat density per unit area. It is known that the heat density per unit area increases with increasing power and, hence, the amount of removed material increases. If the heat input is insufficient to vaporize the material, an amount of melted material re-solidifies in the cavity formed by the interaction between the material and the laser beam. Due to this re-solidification mechanism, a large recast layer occurs in the cavity formed by high power. This large recast layer causes a decrease in crater depth. Figure 4 shows that an increase in the frequency causes an increase in the crater depth and width when the laser power and scan speed are at fixed values. This is one of the reasons for the increase in the number of craters in the present study. Frequency determines the pulse scan overlap rate. Equation (1) and Fig. 2 show the effect of the pulse scan overlap ratio. At 800 mm s^{-1} for two different frequencies, no significant change was observed in the crater formation.

The effect of scan speed on crater formation is shown in Fig. 4. It is observed that the increase in scan speed decreases the crater depth at a constant frequency and laser power. The reason for this reduction can be explained by the interaction time and pulse scan overlap ratio. Laser scan speed affects the pulse overlap rate and the interaction time between laser beam and material. The effect of the interaction time and the amount of heat input is expressed by Eq. (2). The interaction time plays an important role in the amount of heat input transferred to the material from the laser beam. It is clearly seen that the interaction time varies inversely with the scan speed. Accordingly, an increase in scan speed reduces the interaction time, and thus the heat input transferred to the material reduction. When examining Fig. 4, it is clear that the recast layer thickness at 200 mm s^{-1} is higher than at 800 mm s^{-1}, and the conclusion can be drawn that the scan speed significantly affects the recast layer thickness, and consequently also affects the depth of cavity.

Figure 4 also shows the recast layer formation created by the solidification process. The recast layer can clearly be seen at the lower scan speed for all frequencies. Moreover, the recast layer depth shows linearity when laser power is at 30 W. Therefore, examination of the recast layer was performed on samples machined at high power.

When the crater form shown in Fig. 5 is examined, it is seen that the crater depth at the 200 mm s^{-1} is bigger than at the 800 mm s^{-1} for two frequencies. The surface roughness (Ra) profiles and results support this. Therefore, it can be concluded that an increase in scan speed at a constant frequency, or an decrease in frequency at constant scan speed, cause a decrease in the crater depth. Both the SEM and optical microscopy studies showed that a layer distinguishable from the bulk structure was detectable on the subsurface. According to Singh et al. [1], this layer is a re-melted zone, which is a hard brittle layer formed by solidification of the molten metal pool.

Figure 6 shows the recast layer thickness as a function of scan speed and frequency. It can clearly be seen that the recast layer thickness decreases with increasing scan speed and frequency; however, there is sufficiently detectable change that makes a difference when frequency is altered but the scan speed and laser power are fixed. A similar result for the effect of scan speed on recast thickness was reported by Singh et al. [1]. It is reported that this is because the faster the scan, the less time there is for the heat to be conducted into the workpiece and, consequently, it is confined to a smaller region. As reported in a study by Bandyopadhyay et al. [14], the recast layer thickness decreases with increasing pulse frequency, arguing the case that the increased output power at higher pulse frequency enhances the contribution of vaporization to the material removal process and, therefore, reduces the recast layer formation. According to the Wendland et al. [15], a larger overlap will create a higher surface temperature because there will be more pulses hitting each unit area of the target. Moreover, it should be noted that this process is not linear, as heat flux is higher at a higher temperature difference. Effectively, the material removal rate will rise with the overlap, but only to a point where the laser beam creates a grove so deep that molten material cannot escape, so it is re-deposited back onto the substrate. The examination of the recast layer thicknesses showed that they were not uniform, and that they varied between 5–22 μm when the scan speed was 200 mm s^{-1} for all frequencies. Figure 6 also shows that the cavity of craters at 40 kHz is bigger than at 20 kHz for all scan speeds. This affects the recast layer thickness.

Figure 7 shows the various subsurface and surface

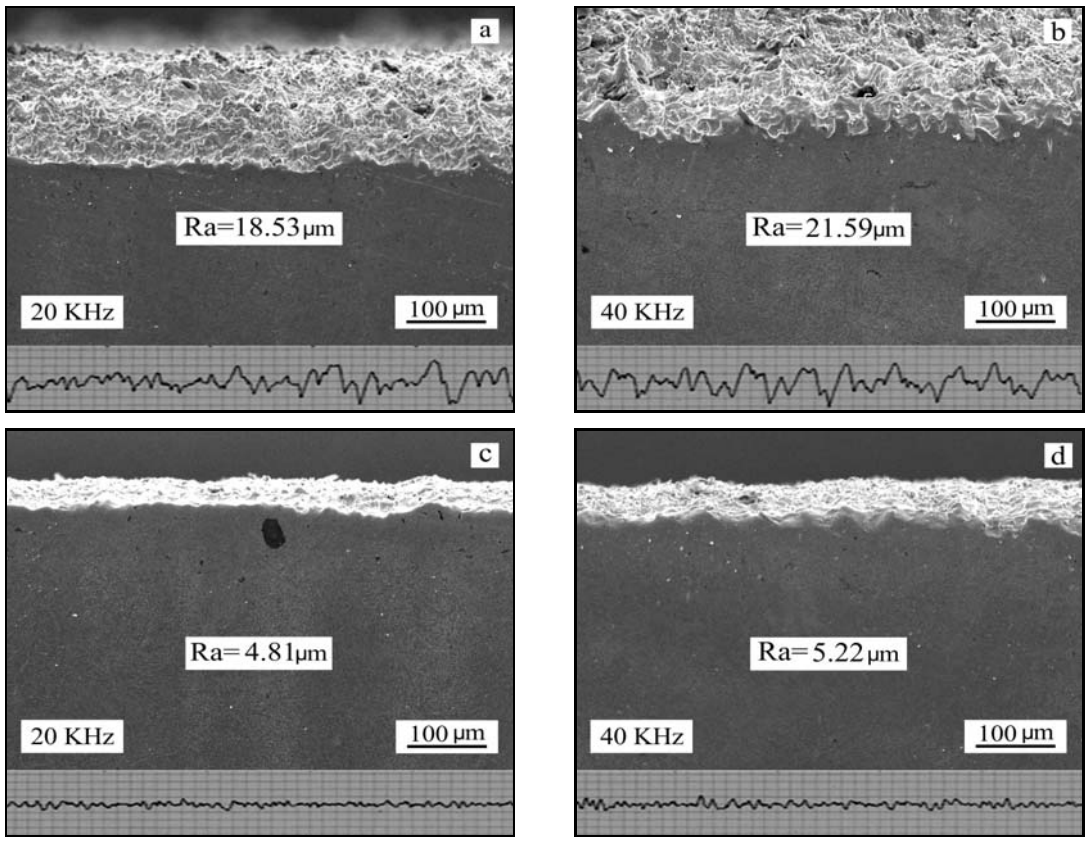

Fig. 5a–d. The surface profiles (a, b – performed at 200 mm s^{-1}; c, d – performed at 800 mm s^{-1}).

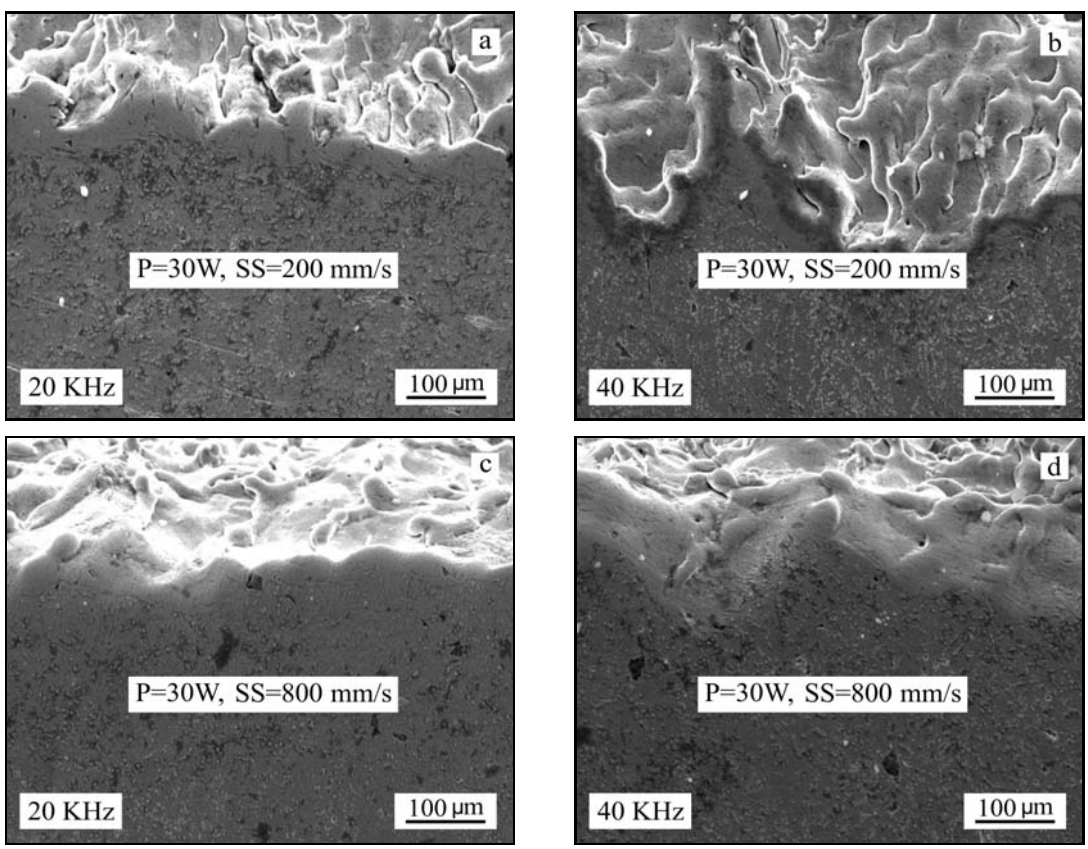

Fig. 6a–d. The recast layer thickness as a function of scan speed and frequency.

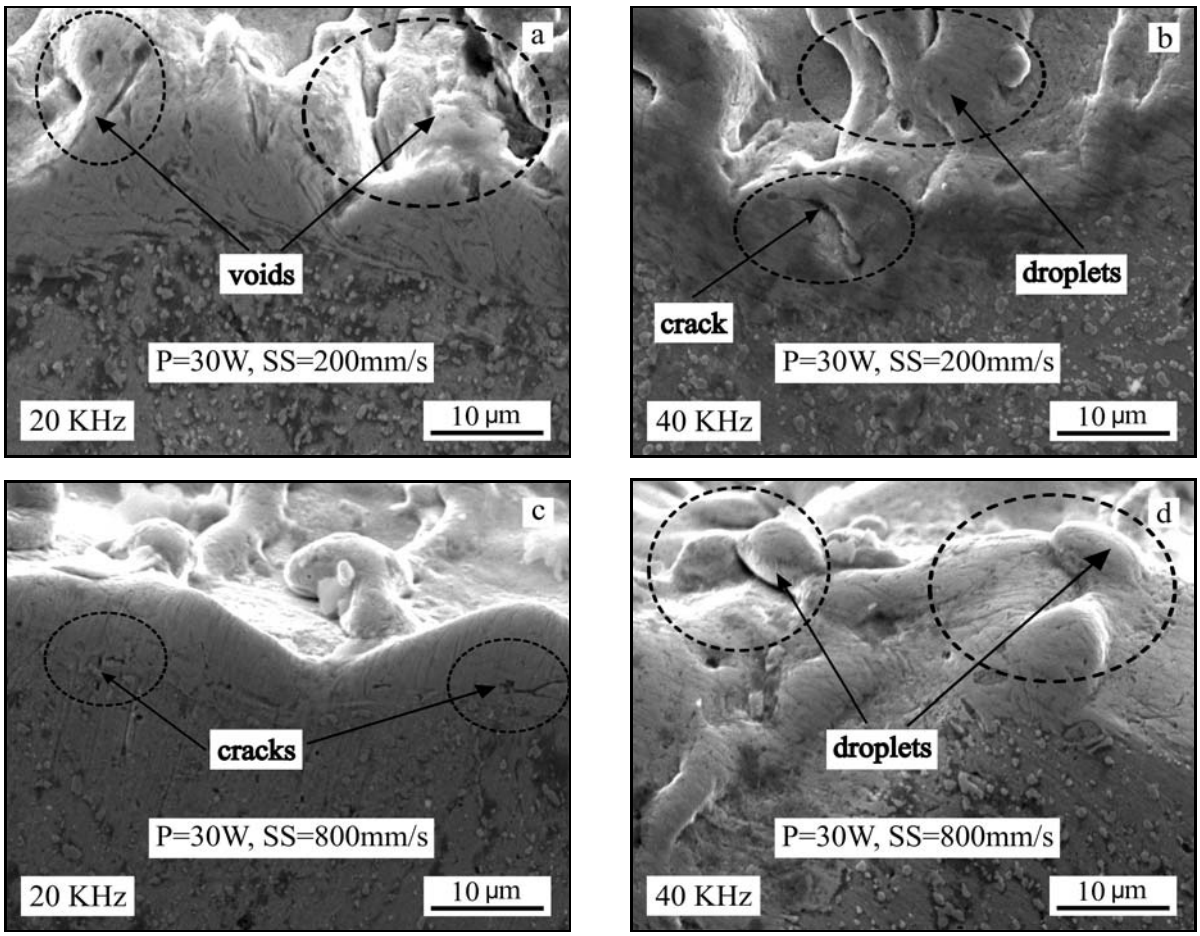

Fig. 7a–d. The subsurface and surface layers.

layers produced by the interaction of scan speed and frequency. It is clearly seen that a large number of micro cracks and voids can be detected on the recast layers of 200 mm s^{-1}. However, the crack and void concentration on the recast layer of 800 mm s^{-1} is less than that at a scan speed of 200 mm s^{-1}. This could be due to the pulse overlap rate. The higher overlap rate produces many craters per unit area that cause nested layers. In the pulsed laser, different cooling rates cause voids and cracks between the recast layers.

4.2. XRD analysis

The phase analysis of the laser machined surface and bulk surface were examined by X-ray diffraction (XRD) with copper (Cu) K_α radiation. The results are shown in Fig. 8. According to the result of the XRD examination, the bulk surface mainly shows that a Fe peak exists on the surface, and the result for the machined surface at two different conditions showed that, in addition to the Fe phase, the $Fe_{2.96}Si_{0.05}O_4$ phase is detected. The presence of this $Fe_{2.96}Si_{0.05}O_4$ phase results from oxidation due to the atmospheric conditions.

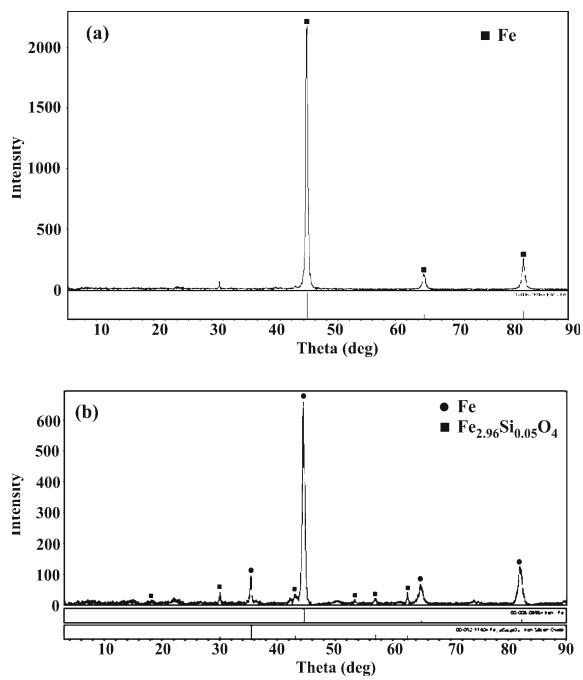

Fig. 8. XRD analysis results for (a) unmachined surface, (b) machined surface.

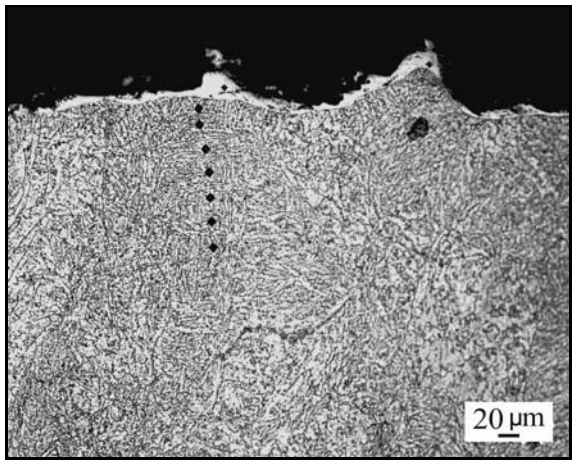

Fig. 9. The trace for hardness.

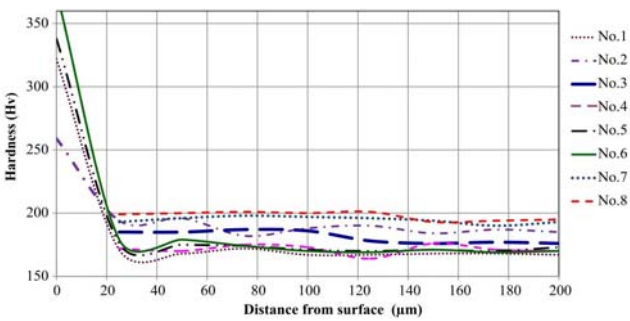

Fig. 10. The hardness results as a function of distance.

4.3. Hardness investigations

Figure 9 shows a sample for the hardness measurement map. At least three measurements were taken on the recast layer where thickness was sufficient to create a hardness trace. However, under some conditions, the recast layer thickness is not large enough to create a hardness trace. Therefore, for these conditions, the first measurement was taken below the recast layer. The hardness distribution as a function of distance was performed using 25 µm distances. The measured hardness trace width was almost 10 µm. Table 3 shows the results of the hardness measurements on the recast layer and below the recast layer. The results for recast layer hardness show that, except for condition 2, the hardness value for all other conditions is similar. This can be explained by the thickness of the recast layer. In this condition, a hardness trace can be created on the recast layer, but the thickness was narrow when compared to other conditions. Therefore, the hardness trace can be affected outside of the recast layer border.

The results showed that a significant change in hardness depending on the distance was not detected for each condition. However, as can clearly be seen, the hardness increases with an increasing scan speed at 30 W. The frequency has not created large differences on the hardness distribution at the constant power and scan speed. Although no sign of microstructure change is evident immediately below and around the laser-scanned region of the workpiece in Fig. 10, the presence of re-melted material on the surface suggests that some microstructure change must have occurred [1]. The hardness results of subsurface as a function of distance support the above results.

5. Conclusions

Microstructure and hardness were examined in the present study. Eight experiments based on laser engraving parameters (laser power, scan speed, frequency) with an optimal value for minimum surface roughness and depth were performed for the investigation. In the machining of AISI H13, the machined surface is characterized by crater formation, while the subsurface is characterized through an optic microscope, SEM, XRD and hardness.

Table 3. The hardness results as a function of distance

No.	Parameters			Hardness, HV Distance from surface (µm)									
	P (W)	SS (mm s^{-1})	F (kHz)	0 µm (recast layer)			25 µm	50 µm	75 µm	100 µm	125 µm	150 µm	175 µm	200 µm
1	18	200	20	321	323	321	171	168	172	167	167	168	168	167
2	18	200	40	260	258	–	194	196	182	188	190	184	187	185
3	18	800	20	narrow layer			185	185	187	186	178	176	177	176
4	18	800	40	narrow layer			172	170	175	173	164	176	171	170
5	30	200	20	323	356	337	176	175	174	171	170	171	170	173
6	30	200	40	417	359	350	179	179	174	170	169	171	169	170
7	30	800	20	narrow layer			193	196	198	197	196	194	190	193
8	30	800	40	narrow layer			199	200	201	200	201	193	194	195

The parameters which significantly affect the recast layer thickness are the power and scan speed. The scan speed at 200 mm s^{-1} produced a higher recast layer thickness and surface roughness (*Ra*) value. Moreover, 30 W of laser power creates a higher recast layer thickness at 40 kHz and 200 mm s^{-1}. The frequency affects the *Ra* and cavity forming. An increase in frequency causes an increase in cavity depth. A higher value of frequency leads to a decrease in the recast layer thickness. The results of XRD analysis clearly showed that, while the bulk surface had a mainly Fe peak, after machining, both Fe and $Fe_{2.96}Si_{0.05}O_4$ phase peaks were detected on the observed surface. The hardness test results indicate that the hardness distribution as a function of distance at each condition does not show a significant variation. However, the recast layer hardness is almost two times higher than the 200 μm distance beneath the recast layer.

Acknowledgements

We are grateful to the Laser Mikron Ltd. Şti. for their support in the experimental studies. This work was financially supported by Ege University under project no. 35MUH30.

References

[1] Singh, R., Melkote, S. N.: International Journal of Machine Tools and Manufacture, *47*, 2007, p. 1139. doi:10.1016/j.ijmachtools.2006.09.004

[2] Melkote, S. N., Kumar, M., Hashimoto, F., Lahoti, G.: CIRP Annals – Manufacturing Technology, *58*, 2009, p. 45.

[3] Dumitru, G., Lüscher, B., Krack, M., Bruneau, S., Hermann, J., Gerbig, Y.: International Journal of Refractory Metals & Hard Materials, *23*, 2009, p. 278. doi:10.1016/j.ijrmhm.2005.04.020

[4] Gilbert, T., Krstic, V. D., Zak, G.: Journal of Materials Processing Technology, *189*, 2007, p. 409. doi:10.1016/j.jmatprotec.2007.02.025

[5] Dubey, A. Kr., Yadava, V.: Journal of Materials Processing Technology, *195*, 2008, p. 15. doi:10.1016/j.jmatprotec.2007.05.041

[6] Mahmoudi, B., Torkamany, M. J., Aghdam, A. R. S. R., Sabbaghzade, J.: Materials and Design, *31*, 2010, p. 2553. doi:10.1016/j.matdes.2009.11.034

[7] Lusquinos, F., Conde, J. C., Bonss, S., Riveiro, A., Quintero, F., Comesana, R., Pou, J.: Applied Surface Science, *254*, 2007, p. 948. doi:10.1016/j.apsusc.2007.07.200

[8] Shin, H. J., Yoo, Y. T., Ahn, D. G., Im, K.: Journal of Materials Processing Technology, *187–188*, 2007, p. 467. doi:10.1016/j.jmatprotec.2006.11.188

[9] Chen, K., Yao, Y. L.: Int J Adv Manuf Technol, *16*, 2000, p. 243. doi:10.1007/s001700050152

[10] Leone, C., Genna, S., Caprino, G., Iorio, I. D.: Journal of Materials Processing Technology, *210*, 2010, p. 1297. doi:10.1016/j.jmatprotec.2010.03.018

[11] Lee, J. H., Jang, J. H., Joo, B. D., Son, Y. M., Moon, Y. H.: Trans. Nonferrous Met. Soc. China, *19*, 2009, p. 917. doi:10.1016/S1003-6326(08)60377-5

[12] Jebbari, N., Jebari, M. M., Saadallah, F., Saugnac, A. T., Bennaceur, R., Longuemard, J. P.: Optics & Laser Technology, *40*, 2008, p. 864. doi:10.1016/j.optlastec.2007.11.006

[13] Kaldos, A., Pieper, H. J., Wolf, E., Krause, M.: Journal of Materials Processing Technology, *155–156*, 2004, p. 1815. doi:10.1016/j.jmatprotec.2004.04.258

[14] Bandyopadhyay, S., Sundar, J. K. S., Sundararajan, G., Joshi, S. V.: Journal of Materials Processing Technology, *127*, 2002, p. 83. doi:10.1016/S0924-0136(02)00270-4

[15] Wendland, J., Harrison, P. M., Henry, M., Brownell, M.: In: Proceedings of 23th International Congress on Application of Lasers & Electro-Optics, Laser Institute of America, Orlando 2005, paper #1901.